Journal of Power Sources 240 (2013) 476–485

Contents lists available at SciVerse ScienceDirect

Journal of Power Sources

journal homepage: www.elsevier.com/locate/jpowsour

Electrochemical performances of a novel high-voltage electrolyte based upon sulfolane and γ-butyrolactone

Xiaoling Cui [a], Hongming Zhang [a], Shiyou Li [a,*], Yangyu Zhao [a], Liping Mao [a], Wei Zhao [a], Yongli Li [a], Xiushen Ye [b]

[a] College of Petrochemical Technology, Lanzhou University of Technology, Lanzhou 730050, China
[b] Qinghai Institute of Salt Lakes, Chinese Academy of Sciences, Xining 810008, China

HIGHLIGHTS

- LiBOB–SL/GBL/DMC electrolyte shows good compatibilities with $LiNi_{0.5}Mn_{1.5}O_4$ and MCMB.
- The electrolyte is an alternative electrolyte for 5 V high-voltage Li-ion battery.
- SL solvent is the main reason for the improvement of electrochemical performance.

ARTICLE INFO

Article history:
Received 14 December 2012
Received in revised form
11 April 2013
Accepted 15 April 2013
Available online 23 April 2013

Keywords:
Lithium-ion battery
Lithium bis(oxalate)borate
Sulfolane
$LiNi_{0.5}Mn_{1.5}O_4$

ABSTRACT

To seek the promising candidate for 5 V electrolytes, fluorine-free lithium bis(oxalato)borat (LiBOB) is chosen as the lithium salt, γ-butyrolactone (GBL) as well as sulfolane (SL) with the property of stability against oxidative decomposition is chosen as supporting electrolyte solvents, and linear diethyl carbonate (DMC) is chosen as the third supporting electrolyte solvent to lower viscosity. After systematical analytical studies, it indicates that SL solvent is the main and key reason for the improvement of electrochemical performance, which not only improves the stability of electrolyte system against oxidative decomposition, but also decreases the electrode polarization resistance. More than that, 1.0 mol L^{-1} LiBOB–SL/GBL/DMC electrolyte shows good compatibilities with both intercalation hosts as $LiNi_{0.5}Mn_{1.5}O_4$ cathode and carbonaceous anode. It suggests that this novel electrolyte would be an alternative electrolyte for 5 V high-voltage rechargeable lithium-ion batteries based upon $LiNi_{0.5}Mn_{1.5}O_4$ cathode.

Crown Copyright © 2013 Published by Elsevier B.V. All rights reserved.

1. Introduction

Since the highest gravimetric and volumetric energy densities, lithium-ion batteries have become one of the most important commercially produced rechargeable batteries [1]. Coupled with developments of electric vehicles (EVs) and hybrid electric vehicles (HEVs), there is an increased demand for lithium-ion batteries with better performance for higher energy and voltage in recent years [2]. The development of 5 V cathode materials and an electrolyte with wide electrochemical window that can provide stable cycling performance at high voltage is of great importance for power battery applications.

$LiNi_{0.5}Mn_{1.5}O_4$ is of high operating potential (4.7 V vs. Li/Li^+) and three dimensional lithium-ion diffusion paths in the spinel lattice, and has been extensively studied as a 5 V cathode material for lithium-ion batteries during the past decade [3–5]. Lithium-ion batteries with $LiNi_{0.5}Mn_{1.5}O_4$-based positive electrodes are expected to provide high power/energy densities for EVs, HEVs and the other large energy storage systems [6].

The electrolyte greatly affects electrochemical performances of $LiNi_{0.5}Mn_{1.5}O_4$-based cells, and the bottleneck effect of electrolyte becomes especially conspicuous in the efforts of developing a coveted "5 V" class Li-ion chemistry [7].

At present, usually the commercial 5 V electrolyte consists of a fluorine-containing lithium salt and alkyl carbonate solvents, for example the lithium hexafluorophosphate ($LiPF_6$)–ethylene carbonate (EC)/diethyl carbonate (DMC) electrolyte system [8–10].

However, the preferred salt, $LiPF_6$, can undergo an autocatalytic decomposition into undesired products as LiF and PF_5. The formed PF_5 is a very strong Lewis acid, and reacts irreversibly with any water present to form HF ($PF_5 + H_2O = PF_3O + 2HF$). HF itself reacts with ROLi (lithium alkoxide) and $ROCO_2Li$ (lithium alky carbonate)

* Corresponding author. Tel.: +86 931 2973305; fax: +86 931 2973648.
E-mail addresses: sylilw@163.com, sylilw@yahoo.com.cn (S. Li).

0378-7753/$ – see front matter Crown Copyright © 2013 Published by Elsevier B.V. All rights reserved.
http://dx.doi.org/10.1016/j.jpowsour.2013.04.063

species on anode material surface to form LiF, alcohol (ROH) and alkyl carbonate ($ROCO_2H$), which are detrimental to form a stable and conductive SEI layer. And to make matters worse, the HF could attack cathode material to make transitional metals dissolved, especially at elevated temperature [11]. These reactions are detrimental to the performance of battery and would lead to safety hazards. Thus, the search for an alternative salt for lithium-ion batteries is necessary to maintain good cycle performances.

Recently, a halogen-free lithium salt named lithium bis(oxalato) borate (LiBOB), has been reported as a promising candidate for lithium-ion batteries. It has several advantages over those traditional salts, including super thermal stability, wide electrochemical stability window, higher compatibility with intercalation hosts as cathode and anode in a lithium-ion battery, no erosion to manganese cathode materials, fluorine-free and non-toxic properties, etc [12]. But LiBOB shows low solubility and inferior conductivity in many solvents (linear alkyl carbonate solvents, for example). In addition, when used in a cell, the SEI layer formed on the surface of carbonaceous anode material has high impedance to severely harm the cryogenic property and discharge capacity of the cell. These weaknesses limit the application of LiBOB.

It is important not only to explore an appropriate lithium salt, but also to use appropriate supporting electrolyte solvents for 5 V electrolytes. EC usually was considered stable against oxidative decomposition in lithium-ion batteries, but in fact it was found to be substantially oxidized far below the intercalation potential, rendering it impossible to load graphite with PF_6^- anions [13]. Another application involves the attempt to identify and synthesize several solvent systems as possible candidates for high-voltage electrolytes. Solvents of ethylmethyl sulfone (EMS), adiponitrile (ADN), and polymer electrolytes (PEs) were used, as supporting electrolyte solvents or additives in 5 V electrolyte systems for lithium-ion batteries [13–15]. However, the high cost of materials and difficulties in synthesis limit the large-scale application in commercialization. Until recently, things have begun to get better. It was found that LiBOB showed high solubility and superior conductivity in γ- butyrolactone (GBL) solvent [16]. GBL is a common solvent with wider liquid temperature range and better thermal stability than almost any alkyl carbonate solvent. The melting point, the boiling point and the flash point of GBL are −44 °C, 204 °C and 101 °C, respectively. Moreover, its high dielectric constant (39.1), low viscosity (1.73 mPa S at 20 °C) and high stability against oxidative decomposition are sufficient for the demand of lithium-ion battery electrolyte. However, GBL aggravates the irreversible capacity associated with the reduction process of BOB anions on carbonaceous anode surface to make a resistive solid electrolyte interphase (SEI) layer [17]. It is detrimental to the performance of battery. But organic sulfites and/or sulfone-based electrolytes may help us solve this problem. It was proved that the use of organic sulfites (such as dimethyl sulfite (DMS), diethyl sulfite (DES), ethyl sulfite (ES), propylene sulfite (PS), vinyl ethylene sulfite (VES) and so on) could effectively reduce impedance of the SEI layer on carbonaceous anode surface [18–22]. But their low stabilities against oxidative decomposition limit the application in 5 V electrolytes [19,21]. So, sulfone-based electrolytes, especially sulfolane (SL)-based solvents may the alternative electrolytes for lithium-ion batteries [13,18,22]. SL is a sort of sulfones organic solvent known to with high dielectric constant (43.4), high flash point (166 °C) and high stability against oxidative decomposition (>6.35 V). The use of the electrolyte based on SL in lithium-ion batteries, which shows high stability against oxidative decomposition, satisfactory conductivity and excellent film-forming characteristic, has been reported in our previous study [18,22].

Therefore, in this report, to seek the promising candidate for 5 V electrolytes, fluorine-free LiBOB was chosen as the lithium salt to reduce release of acidic compounds, GBL with the property of high stability against oxidative decomposition was chosen as one of the supporting electrolyte solvents to improve the solubility and conductivity of LiBOB-based electrolyte, SL with the property of high stability against oxidative decomposition was chosen as the second supporting electrolyte solvents to reduce impedance of the cell, and DMC with the property of low viscosity was used as the third supporting electrolyte solvents on the basis of complementary advantages. And systematically analytical studies were carried out on electrochemical performances of this novel electrolyte system. Moreover, to present thorough discussions on electrochemical performances of this novel electrolyte system and the positive role of SL in this system, the electrochemical performances of systems of $LiPF_6$–EC/DMC (the most typical electrolyte system) and LiBOB–GBL/DMC were studied as frame of references.

2. Experimental

LiBOB was synthesized in laboratory by a compressing dry granulation method as described previously [18]. Alkyl carbonate solvent DMC was produced by Zhangjiagang Guotai Huarong New Chemical Materials Co., Ltd. SL was produced by Liaoyang Guanghua Chemical Co., Ltd., and GBL was purchased from Aladdin Reagent Database Inc, both of which were dried by 0.4 nm molecular sieves and alkali metals for at least two days until the water content was typically less than 10 ppm determined by Karl Fischer titration. Electrolyte systems were prepared in an argon atmosphere glove box by dissolving 1.0 mol L^{-1} LiBOB in two kinds of solvent mixtures, SL/GBL/DMC and GBL/DMC, with the volume ratio of 1:1:1 and 1:1, respectively. 1.0 mol L^{-1} $LiPF_6$–EC/DMC (1:1), which was used as a control electrolyte, was purchased from Zhangjiagang Guotai Huarong New Chemical Materials Co., Ltd.

The negative electrode was composed of 92 wt.% MCMB and 8 wt.% poly (vinylidene fluoride) (PVDF). The positive electrode was composed of 84 wt.% $LiNi_{0.5}Mn_{1.5}O_4$, 8 wt.% acetylene black and 8 wt.% PVDF.

Experimental cells were assembled in an argon atmosphere glove box using a lithium sheet as the anode material, one of the above prepared electrodes as the cathode material, one of the above mentioned electrolytes as the electrolyte material, and a Celgard (2400) porous polypropylene as the separator material.

Ionic conductivities of the electrolytes were measured by a DDSJ-308A conductivity meter (Shanghai, China) in a temperature range of 243.15–333.15 K.

Electrochemical windows of the electrolytes were measured in a three-electrode system (the negative electrode was used as the working electrode with a reaction area of 1 cm^2, and lithium sheets were used both as the counter electrode and the reference electrode, respectively) for the cyclic voltammetry (CV), through a CHI660C Electrochemical Workstation (Shanghai, China) at the scan rate of 2 mV s^{-1} in the voltage range of 3.0–6.0 V.

The positive electrodes before cycle were put into 3.0 mL sealed vials filled with 1.0 mol L^{-1} LiBOB–SL/GBL/DMC and 1.0 mol L^{-1} $LiPF_6$–EC/DMC electrolytes for two months, respectively. Then the concentrations of the transition-metal ions in different electrolytes were obtained by IRIS Advantage Inductively Coupled Plasma-Atomic Emission Spectrometry (ICP-AES) measurement (United States).

Electrochemical impedance spectroscopy (EIS) spectra of the Li/MCMB cells with different electrolytes were measured on a three-electrode electrochemical workstation, at 0.003 V during the initial lithiation process at room temperature. The negative electrode was used as the working electrode, and lithium sheets were used both as the counter electrode and the reference electrode, respectively. All of the electrode areas are 1 cm^2, respectively. A

sinusoidal AC perturbation of 5 mV was applied to the electrode over the frequency range of 100 kHz to 0.01 Hz.

Carbonaceous anode materials of the experimental cells were stripped off from carbon electrodes in an Ar glove box after 10 cycles. Prior to surface analysis, the anode materials were rinsed with DMC three times to remove adsorbed substances, and then dried in a vacuum drying even for 12 h at room temperature to remove the residual solvent of DMC.

The morphologies and sections of SEI layers on anode material surfaces in Li/MCMB cells were observed under a JSM-5600 scanning electron microscope (SEM, Japan).

Electrochemical measurements of the cells were carried out on a LAND CT2001A tester (Wuhan, China) in different voltage ranges of 0.003–2 V for Li/MCMB cells, and 3.5–5.0 V for $LiNi_{0.5}Mn_{1.5}O_4$/Li cells.

All the calculations had been performed by the Gaussian 09 program package [23]. The geometry optimizations of EC, GBL, DMC and SL were carried out with the DFT models and the B3LYP method with 6-31 + G (d, p) basis set. The total energies and frontier molecular orbital energies of organic molecules were calculated. Moreover, the equilibrium and transition structures of reductive dissociation processes of GBL, SL and LiBOB were fully optimized at the same level.

3. Results and discussion

3.1. Ionic conductivities of three different electrolytes

To study the effect of conductivity on temperature, graphs for three different electrolytes were plotted and depicted in Fig. 1. Fortunately, the maximum solubility of LiBOB in pure GBL is about 2.5 M at room temperature, which would greatly improve the solubility and conductivity of LiBOB–GBL/DMC and LiBOB–SL/GBL/DMC electrolytes. As a result, the conductivity of every electrolyte is higher than that of common LiBOB-based system [18,24]. Although conductivities of LiBOB–GBL/DMC and LiBOB–SL/GBL/DMC electrolytes are greatly improved, from 263.15 K to 333.15 K, each of them is still lower than that of $LiPF_6$–EC/DMC system, especially at high temperature, while each of these electrolytes can meet the requirements of lithium-ion batteries over a wide range of temperature. The low conductivity is mainly due to the fact that the electrolyte based upon LiBOB has higher viscosity than the one based upon $LiPF_6$. Similarly, the conductivity of LiBOB–SL/GBL/DMC system is lower than that of LiBOB–GBL/DMC system, as a result of the high viscosity of SL.

It is obvious that low temperature performance of $LiPF_6$–EC/DMC system is poorer than those of LiBOB–GBL/DMC and LiBOB–SL/GBL/DMC systems, respectively. Trace of solid material emerges from the $LiPF_6$–EC/DMC electrolyte just at 253.15 K, and the precipitation becomes more and more with the temperature decreasing. The result may be due to the higher melting point of EC (about 38 °C) than SL (about 27 °C) and GBL (about −44 °C), respectively.

3.2. Electrochemical stabilities of three different electrolytes

Electrochemical stabilities of the three electrolytes are investigated by CV measurement. The results are shown in Fig. 2. It indicates that, when the anodic potential is high enough, the oxidation reactions will happen. Current densities would start to increase dramatically when potentials are higher than 5.0 V, 5.2 V and 5.5 V, corresponding to LiBOB–GBL/DMC, $LiPF_6$–EC/DMC and LiBOB–SL/GBL/DMC systems, respectively. And the most likely reason for the oxidation reaction is due to the decomposition of lithium salt, since the fact that the decomposition potential of LiBOB–GBL/DMC electrolyte is lower than that of the corresponding supporting solvent as GBL/DMC (~6.0 V). The result also indicates that the originally less stable LiBOB–GBL/DMC system is stabilized by the presence of SL. That is to say, SL is able to improve the stability of electrolyte system against oxidative decomposition, which is very useful in a 5.0 V anode intercalation device. Presumably the unique anodic stability is due to the formation of an effective protective film on the cathode surface [13].

Based upon the molecular orbital theory, the ability to gain and lose electrons is judged by the energy level of the highest occupied molecular orbital (HOMO) and the lowest unoccupied molecular orbital (LUMO) [25,26]. The total energies (E_T), the frontier molecular orbital energies ($E/_{HOMO}$ and $E/_{LUMO}$), and the energy gaps (Δ^*) between the HOMO and the LUMO of GBL, DMC and SL molecules are calculated and listed in Table 1, respectively. It is obvious that the HOMO energy as well as the total energy of GBL molecule is generally higher than that of SL and DMC molecules, respectively. It indicates that GBL molecule should be a better electron donor than any other organic molecule, which will be oxidized behind SL and DMC molecules. In other words, based upon the calculation, it can be speculated that the stability of LiBOB–GBL/DMC system against

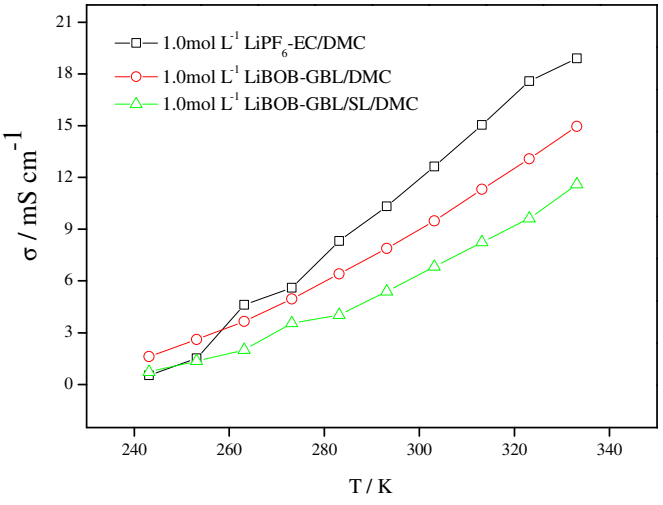

Fig. 1. The dependence of ionic conductivity on temperature for three different electrolytes over the temperature range from 243.15 K to 333.15 K.

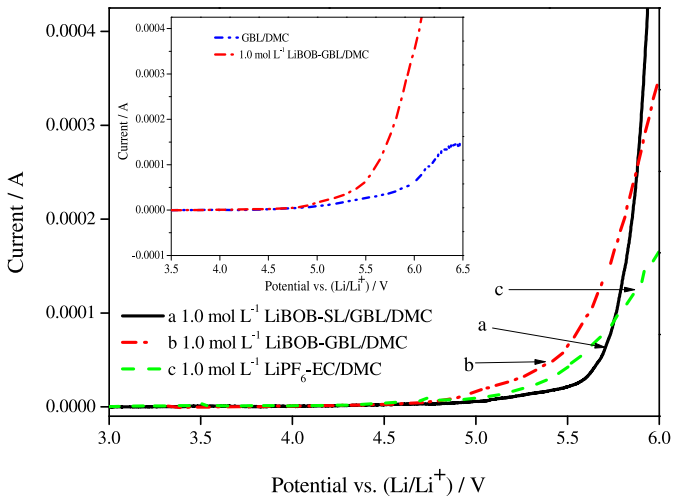

Fig. 2. Current potential curves of different electrolytes at a scan rate of 5 mV s^{-1} in the range of 3.0–6.0 V at room temperature.

Table 1
Total energies and frontier molecular orbital energies of SL, GBL and DMC molecules, respectively.

Organic molecule	E_T/Ha	Frontier molecular orbital energy/Ha		
		E/HOMO	E/LUMO	ΔE_g^{a*}
SL	−705.72336	−0.28800	−0.01225	0.27575
GBL	−306.415768	−0.27959	−0.00643	0.27316
DMC	−343.535757	−0.29984	0.00477	0.30461

$\Delta E_g^{a*} = E/_{LUMO} - E/_{HOMO}$.

oxidative decomposition should be higher than that of $LiPF_6$–EC/DMC system. But that does not match with the conclusion shown in Fig. 2. This is a further proof of the unique anodic stability of SL. Presumably the sulfur-containing compounds produced by electrochemical oxidation of SL will precipitate on the surface of cathode material, and the further oxidation processes would be effectively attenuated.

3.3. The concentrations of the transition-metal ions in different electrolytes

To investigate the possible dissolution of the spinel into the electrolyte, the positive electrodes before cycle were put into 3.0 ml sealed vials filled with 1.0 mol L^{-1} LiBOB–SL/GBL/DMC and 1.0 mol L^{-1} $LiPF_6$–EC/DMC electrolytes for two months, respectively. Then the contents of Mn and Ni elements in electrolyte solutions were measured by ICP analysis. The results are listed in Table 2. It is obvious that the contents of Mn and Ni elements in $LiPF_6$–EC/DMC electrolyte are extremely lager than those in LiBOB–SL/GBL/DMC electrolyte, respectively. In other words, 1.0 mol L^{-1} LiBOB–SL/GBL/DMC electrolyte shows better compatibility with $LiNi_{0.5}Mn_{1.5}O_4$ active material than 1.0 mol L^{-1} $LiPF_6$–EC/DMC electrolyte. The reason is that, $LiPF_6$–EC/DMC electrolyte tends to produce protonic acids, such as HF, which would locally cause the dissolution of Mn and Ni elements from $LiNi_{0.5}Mn_{1.5}O_4$ active material [27]. It indicates that the novel electrolyte, 1.0 mol L^{-1} LiBOB–SL/GBL/DMC, would be an alternative electrolyte for 5 V high-voltage rechargeable lithium-ion batteries based upon $LiNi_{0.5}Mn_{1.5}O_4$ cathode.

3.4. Electrochemical characteristics of the first cycle of Li/MCMB cells

The first charge and discharge curves of Li/MCMB half-cells with three different electrolyte systems are given in Fig. 3a. It can be seen that the discharge processes are quite different from each other, though each one has three plateaus. The first plateau is very obvious in the voltage range of 1.8–1.6 V for LiBOB-based cells, and is not instantly discernible in the voltage range of 1.4–1.2 V for $LiPF_6$-based cell, during the initial lithiation process. Correspondingly, a 1.76 V reductive peak for LiBOB–GBL/DMC system, a 1.70 V reductive peak for LiBOB–SL/GBL/DMC system, and a tiny 1.30 V reductive peak for $LiPF_6$-EC/DMC system are given in Fig. 3b. The well-known reason is that, the reductive plateau of every LiBOB-based cell arises from the reduction of BOB anions which plays an active role in the formation of a preliminary unstable SEI layer, while the reductive plateau of $LiPF_6$-based cell is associated with

Table 2
ICP results of the dissolution of transition-metal ions in the electrolyte solution.

Samples	Mn (ppm)	Ni (ppm)
LiBOB–SL/GBL/DMC	2.102	0.470
$LiPF_6$–EC/DMC	505.9	110.3

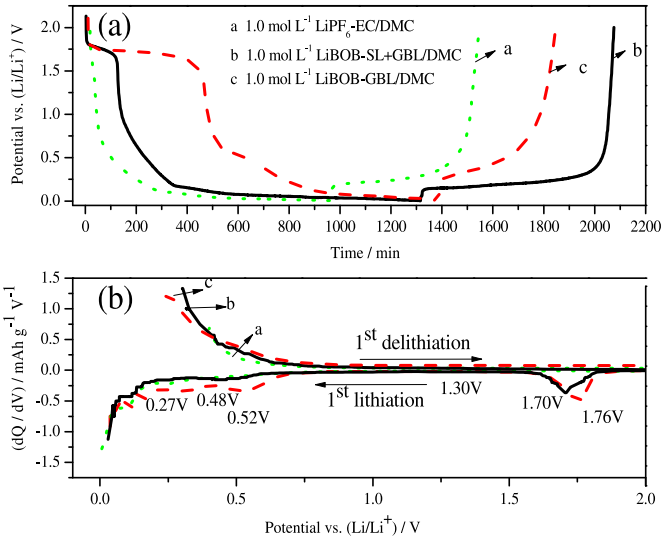

Fig. 3. (a) The first charge and discharge curves and (b) differential capacity plots of Li/MCMB cells with three different electrolytes.

little inserted EC [28]. But even more than that, there are other reasons as well for the reductive plateau of LiBOB-based cells in the voltage range of 1.8–1.6 V, for the fact that there are marked differences across not only decomposition potentials, but also peak areas, between LiBOB–SL/GBL/DMC and LiBOB–GBL/DMC systems. As shown in Fig. 3, when mixed with the supporting electrolyte solvent of SL, both the decomposition potential and the percentage integral area (or the plateau length) would decrease. It indicates that the reductive plateau about 1.7 V arise not only from the reduction of BOB^- anions, but also from the reduction of solvent, which plays an active role in the formation of a more effective SEI film [29].

In order to verify the effect of solvent, the initial discharge curves of Li/MCMB half-cells with GBL/diethyl carbonate (DEC) and SL/DEC solvent systems are studied, respectively (DEC was chosen for its low viscosity and low melting point, to lower viscosities and increase wettabilities of GBL and SL, respectively). The results are shown in Fig. 4. It can be seen that reductions of SL and GBL would be taken place at about 1.64 V and 1.1 V, respectively. And the

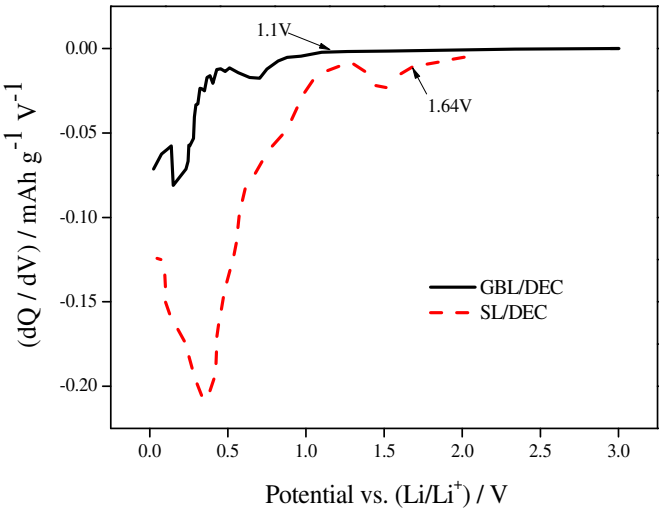

Fig. 4. Differential capacity plots of Li/MCMB cells with two different solvent systems during the initial lithiation process.

reduction of SL solvent is more obvious. It means that the supporting electrolyte solvent of SL has high reductive potential, and will be reduced during the first plateau stage in Fig. 3a. So, for the cell with LiBOB–SL/GBL/DMC electrolyte, except from BOB anions, SL would be involved in the first reductive plateau to form a more effective SEI film. And this would result in the decrease of both of the decomposition potential and the percentage integral area (or the plateau length) in Fig. 3.

To further verify the conclusion, the LOMO energies and the total energies of GBL, DMC and SL molecules should be put into use, as shown in Table 1. It is evident that the LUMO energy as well as the total energy of SL molecule is generally lower than that of GBL and DMC molecules, respectively. It indicates that SL molecule will be reduced prior to GBL and DMC molecules during the first lithiation process. In other words, presumably the sulfur-containing compounds produced by the electrochemical reduction of SL would precipitate on the surface of anode material prior to GBL and DMC in LiBOB–SL/GBL/DMC electrolyte, and the further reduction processes would be effectively attenuated. This is consistent well with the inference getting from Fig. 3.

As shown in Fig. 3a, the second plateau is, respectively, presented in the voltage range of 1.0–0.1 V in every electrolyte system. Correspondingly, a 0.52 V reductive peak for LiBOB–GBL/DMC system, a 0.48 V reductive peak for LiBOB–SL/GBL/DMC system, and a 0.27 V reductive peak for $LiPF_6$–EC/DMC system are given in Fig. 3b. This plateau is associated with the irreversible reductions of both electrolyte components and surface chemical groups of graphite, and the resulting SEI layer will be structurally dense and stable. As shown in Fig. 4, the decomposition potential of each of LiBOB-based cells is higher than that of $LiPF_6$-based cell, for the reduction of GBL solvent. And in Fig. 3b, it shows the percentage integral area of electrolyte system is in the order of LiBOB–GBL/DMC > LiBOB–SL/GBL/DMC > $LiPF_6$–EC/DMC. The results indicate that (1) though preliminary SEI layers are formed on surfaces of carbonaceous anode materials in LiBOB-based cells, the irreversible reductions could not be effectively reduced, and (2) when mixed with the supporting electrolyte solvent of SL, the reduction of SL in the first plateau is able to decrease the reduction of other solvents in the second plateau.

For each of the electrolytes, the well-known intercalation of Li^+ ions into graphite occurs below 0.1 V, which is associated with the third plateau in Fig. 3a, and the end of the elevation in Fig. 3b.

From Fig. 3, studies also have shown that cells based upon LiBOB should take more energy to form SEI layers. The initial charge–discharge efficiency of the cell with $LiPF_6$–EC/DMC, LiBOB–GBL/DMC and LiBOB–SL/GBL/DMC electrolyte systems are about 62.0% (the charge and discharge capacities are 215.1 mAh g^{-1} and 346.8 mAh g^{-1}, respectively), 50.7% (the charge and discharge capacities are 212.2 mAh g^{-1} and 424.8 mAh g^{-1}, respectively) and 57.5% (with the charge and discharge capacities are 241.8 mAh g^{-1} and 420.4 mAh g^{-1}, respectively). Typically, taking more energy to form a SEI layer simply means that amounts of limited Li^+ ions would be consumed in the initial forming cycle, and the resulting SEI layer would be denser or thicker to increase the impedance of the cell. That is considered bad for the cryogenic property and discharge capacity of a lithium-ion battery. Fortunately, despite these weaknesses, LiBOB–SL/GBL/DMC electrolyte shows good electrochemical performances, as shown in the latter part of this paper. On one hand, the content of Li^+ ions could reach 1 mol L^{-1}, which benefits from the supporting electrolyte solvent of GBL. And that is higher than the maximum solubility of LiBOB in typical carbonate mixtures, usually as 0.7 mol L^{-1} or 0.8 mol L^{-1} [30]. Thus, the source of Li^+ ions is relatively sufficient. On the other hand, though the SEI layer is denser and thicker, the impedance of the cell with LiBOB–SL/GBL/DMC electrolyte is lower than that of the cell with $LiPF_6$-EC/DMC electrolyte, which benefits from the supporting electrolyte solvent of SL that will be reduced to produce good conductors of Li^+ ions. This will be discussed in detail later on. Besides, the fact that LiBOB–SL/GBL/DMC electrolyte takes less energy to form a SEI layer than LiBOB–GBL/DMC electrolyte is further proof of the unique passive property of SL to decrease the reduction of solvents.

Further studies show that the prior two plateaus are the main reason that cells based upon LiBOB take more energies to form SEI layers. The total irreversible energies spent in the prior two plateaus are about 138.7 mAh g^{-1}, 107.7 mAh g^{-1} and 74.6 mAh g^{-1}, for cells based upon LiBOB–GBL/DMC, LiBOB–SL/GBL/DMC and $LiPF_6$–EC/DMC electrolytes, respectively.

Fig. 5 shows differential capacity plots of Li/MCMB cells with different electrolytes during the second cycle. It reflect that, the prior two plateaus can be apparently observed only in the initial graphite-lithiation cycle due to the self-limiting nature of SEI layer growth on graphite, while the third plateau is reversible and reproducible in the subsequent cycles, and the corresponding total charge capacity would be approximately equal to the total discharge capacity.

3.5. SEM measurement of MCMB surface in Li/MCMB cells

The SEM spectra of surfaces and sections of carbonaceous anode materials in Li/MCMB cells with three electrolytes are shown in Fig. 6, respectively. It indicates that there are obvious SEI layers on the anode surfaces with some morphology differences. In Fig. 6a_1 and b_1, the morphological anode electrodes with LiBOB–GBL/DMC as well as LiBOB–SL/GBL/DMC electrolyte are completely covered by a more compact and thicker SEI layer than that with $LiPF_6$–EC/DMC electrolyte (Fig. 6c_1), the surface of which is rough and irregular. The difference arises from different formation and decomposition mechanisms of SEI layers. As have been discussed before, formation processes of SEI layers on LiBOB-based electrodes, respectively, include two stages with reductions of LiBOB salt and organic solvents, while the formation process of SEI layer on $LiPF_6$-based electrode nearly include only one stage with reductions of alkyl carbonates.

For structures of SEI layers on cross-sections, as shown in Fig. 6a_2, b_2 and c_2, each of the ones with LiBOB-based electrolytes is much thicker, denser and more compact than the one with $LiPF_6$-based electrolyte. It is good for the protective effect of carbonaceous

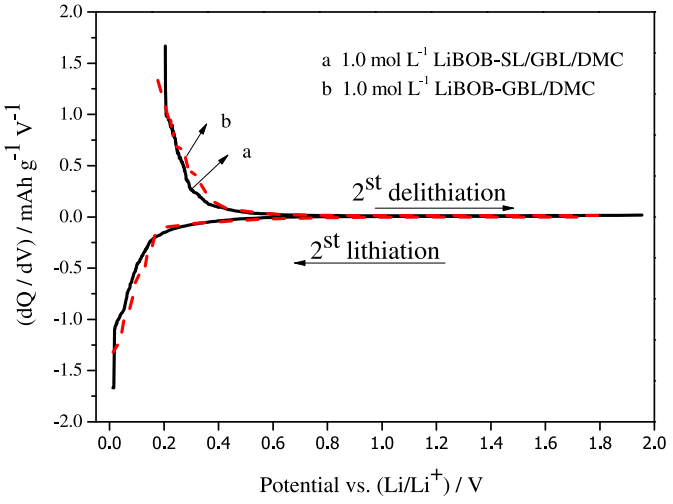

Fig. 5. Differential capacity plots of Li/MCMB cells with different electrolytes during the second cycle.

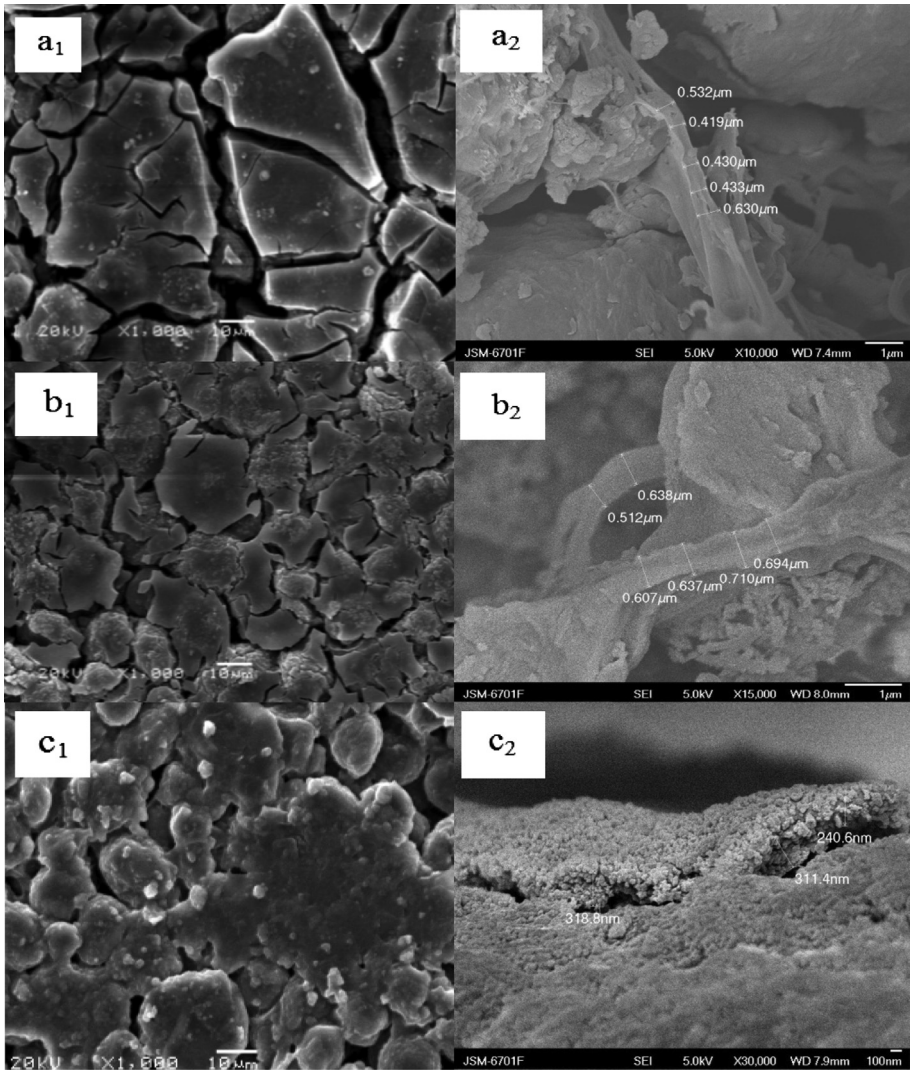

Fig. 6. The SEM spectra of surfaces and sections of graphite cathodes with three electrolytes after 10 cycles: (a_1 and a_2) 1.0 mol L^{-1} LiBOB–GBL/DMC; (b_1 and b_2) 1.0 mol L^{-1} LiBOB–SL/GBL/DMC; and (c_1 and c_2) 1.0 mol L^{-1} $LiPF_6$–EC/DEC.

anode material, but may cause the increasing of impedance. Fortunately, the cell with LiBOB–SL/GBL/DMC electrolyte shows low impedance than the cell with the most typical electrolyte system of $LiPF_6$–EC/DMC. That will be discussed in detail later on.

3.6. DFT calculations on the decomposition of GBL and LiBOB

In order to distinguish the species of decomposition compounds, optimized structures and binding energies of the possible electrochemical reduction processes are shown in Figs. 7–9, respectively. Every ΔE value is defined as the energy change in the reaction process.

As shown in Fig. 7, a GBL molecule initially turns into the ion-pair intermediate product (2), when a Li^+ ion would tend to coordinate with the most electronegative O atom. Then an electron would be transferred from anode to intermediate product (2) to form the intermediate product (3). With the presence of another Li^+ ion and another electron, the intermediate product (3) leads to the formation of intermediate products (4) and (5) in order. Finally, two compounds, $LiCH_2COOLi$ (compound 6), and $CH_2{=}CH_2$ (compound 7), are produced followed by the dissociation of intermediate product (5) [31]. Perhaps the formation of a barrier-free self-dimerizing complex ($(LiCH_2COOLi)_2Li$, compound 8) would also occur within two intermediate products of (6). It deduces that the decomposition compounds for GBL may include $LiCH_2COOLi$, $(LiCH_2COOLi)_2Li$, and so on.

The DFT calculation is a further proof that the reduction of LiBOB salt and SL solvent would occur at the same level. The optimized geometry and selected structural parameter of LiBOB salt at B3LYP/6-311 + G(d,p) level are presented in Fig. 8. Two different structures are acquired since the atom of Li could coordinate with different oxygen atoms, as labeled LiBOB-1 and LiBOB-2, respectively. The relative energy of LiBOB-1 is −786.838 Ha, which is slightly lower than that of LiBOB-2 (−786.816 Ha), it suggests that LiBOB-1 is more stable than LiBOB-2, which differs from the viewpoint of Huang [32].

As shown in Fig. 9, the initial reductive decomposition of the LiBOB-1 involves one electron transfer from anode to a LiBOB molecule, resulting in a radical anion $[LiBOB]^-$ (intermediate product (9)). The ring-opening reaction of the radical anion $[LiBOB]^-$ would proceed via further combination with another Li^+ ion to generate a complex intermediate product (10). Then the resulting intermediate product (10) would couple with an SL molecule and a Li atom to change into intermediate product (11). Finally, with the presence of two Li atoms, the intermediate product (11) leads to the formation of $Li_2C_2O_4$, SO_2, C_4H_8, as well as a $Li(BC_2O_4)_n$ polymer.

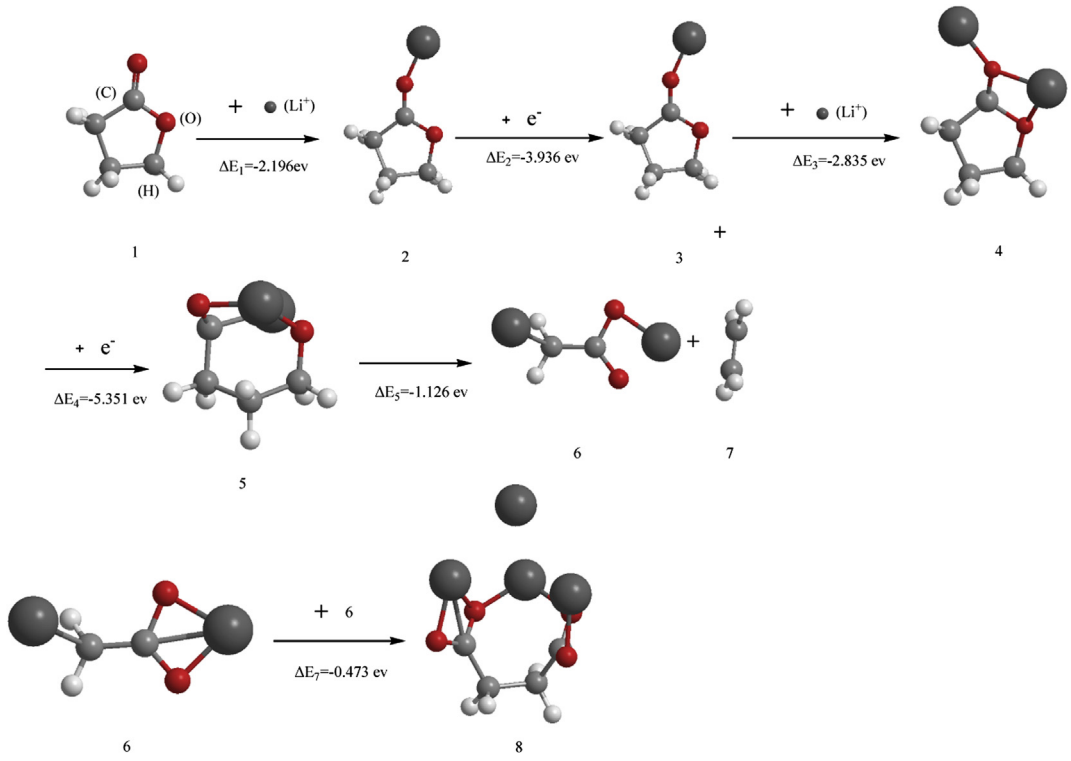

Fig. 7. The B3LYP optimized geometries and ΔE_1, ΔE_2, ΔE_3, ΔE_4, ΔE_5 and ΔE_6 values for the GBL–Li_n complexes ($n = 0$, 1 and 2).

3.7. FTIR measurements of the SEI layers on surfaces of carbonaceous anode materials

Fig. 10 shows the FTIR spectra of the SEI layer on the anode material in Li/MCMB cell at different potentials, cycled with 1.0 mol L^{-1} LiBOB–SL/GBL/DMC electrolyte during the initial cycle. Even at 1.5 V, the reduction of LiBOB salt and SL solvent would occur. The peaks emerging around 1298.7 cm^{-1}, 1255.87 cm^{-1}, 1148.9 cm^{-1}, 1141 cm^{-1}, 905.4 cm^{-1}, 733.5 cm^{-1} and 563.2 cm^{-1} are attributed to the decomposition products of SL solvent [33]. The presence of lithium oxalate is supported by a peak at 1650 cm^{-1}. And at 1.0 V, the reduction of GBL solvent would occur, for new absorption peaks appear at 1420 cm^{-1} and 1040 cm^{-1}, which are characteristics of lithium carbonates and lithium carboxylates, respectively. The lithium carbonates are converted from lithium carboxylates, with the fact that lithium carboxylates are highly sensitive to CO_2 and water. These phenomena are in good agreement with theoretical calculation results and discussions before.

3.8. EIS analyses of negative electrodes

EIS spectra are widely used to investigate electrolyte–electrode reactions, such as interface electrochemical reactions and the subsequent formation of SEI films. Impedance correlations of the negative electrodes, which are plotted on the basis of the data of the initial lithiation processes of Li/MCMB half-cells with three electrolyte systems, are given in Fig. 11. The EIS spectra of the cells are usually described by four major features. High frequency and medium frequency flat semicircles can be attributed to surface films (R_f) and interfacial charge-transfer (R_{ct}), respectively (coupled with film and/or interfacial capacitances). A low frequency "Warburg"-type element reflects the solid state diffusion of Li^+ ions and finally. And at the very low frequency, the Z' versus Z'' plot becomes a steep, nearly vertical line, which reflects the capacitive behavior of the electrode (Li^+ ions insertion and corresponding charge-transfer). It is clearly indicated that the cell with LiBOB–SL/GBL/DMC electrolyte has the lowest impedance of SEI layer, and the one with LiBOB–GBL/DMC electrolyte has the highest impedance of SEI layer. It means that LiBOB–GBL/DMC electrolyte could overcome the bottleneck effect as high impedance of typical LiBOB-based cell.

However, it might be counter-intuitive to some extent. As we shown in Fig. 3, each of the cells based upon LiBOB electrolytes takes more energy to form an effective SEI layer, mainly arising from large amounts of reductions of BOB^- anions and organic solvents, which will typically lead to a thick SEI layer with high impedance. Based on our studies and experiences, we make inferences about the impedance reduction of LiBOB–SL/GBL/DMC electrolyte as follows, (1) the resulting SEI layer based upon LiBOB–SL/GBL/DMC electrolyte is denser and more uniform than the one based upon $LiPF_6$–EC/DMC electrolyte, which would benefit for the uniform transportation of Li^+ ions, and (2) many compounds containing S element are produced in SEI layer for the reductions of SL, and these compounds are better conductors of Li^+ ions than analogical carbonates, which sharply favor the impedance reduction. On the whole, the electrochemical performance of lithium-ion battery is highly dependent on the SEI film of carbon electrode, and LiBOB–SL/GBL/DMC electrolyte can conduct a more promising candidate than $LiPF_6$–EC/DMC electrolyte.

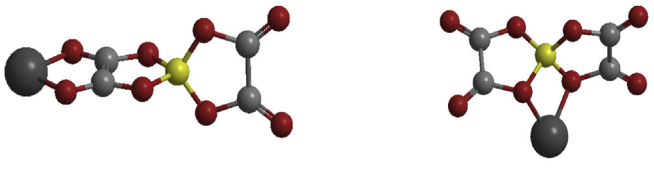

Fig. 8. The optimized geometry of LiBOB salt at B3LYP/6-311 + G(d,p) level.

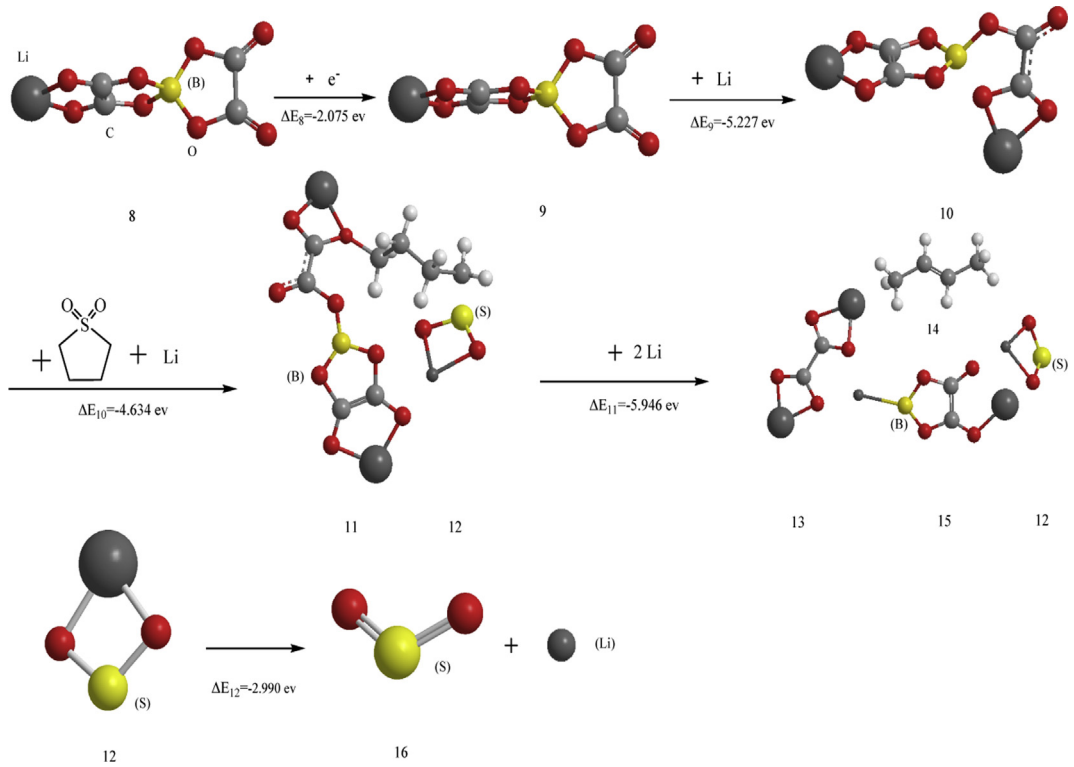

Fig. 9. The B3LYP optimized geometries and ΔE_7, ΔE_8, ΔE_9, ΔE_{10} and ΔE_{11} values for the LiBOB complexes.

3.9. Cycle performances of $LiNi_{0.5}Mn_{1.5}O_4$/Li cells

The capacity loss of a Li-ion cell during cycle is mainly caused by both the lithium loss resulted from lithium-consuming SEI layer growth and the rate capability loss mostly due to the rise of interfacial resistance [34,35]. Fig. 12 shows the cycling performances of $LiNi_{0.5}Mn_{1.5}O_4$/Li half-cells with three electrolytes with 0.5 C of discharge rate at room temperatures, respectively. It is obvious that the capacity of the cell with LiBOB–GBL/DMC electrolyte decreases extremely fast, which initially delivers 121.3 mAh g^{-1} and only retains 73.1 mAh g^{-1} at the 28th cycle. That may be caused by the bottleneck effect of electrolyte which is unstable at high potential. The capacity retention efficiency of the cell with $LiPF_6$–EC/DMC is improved, but still remains limited, for reactions between $LiNi_{0.5}Mn_{1.5}O_4$ cathode material and the inevitable protonic acids, such as HF. Fortunately, the cell with LiBOB–SL/GBL/DMC electrolyte shows good cycle performance, which benefits from the specially selected lithium salt and supporting electrolyte solvents. It can be observed that after 100 cycles, the discharge capacity retention efficiency of the cell with LiBOB–SL/GBL/DMC electrolyte is 85.9%, which is higher than that of the cell with $LiPF_6$–EC/DMC electrolyte (77.6%).

Mean voltage, the voltage at half time of the cells' running, reflects how long the cells can run under normal work voltage. As

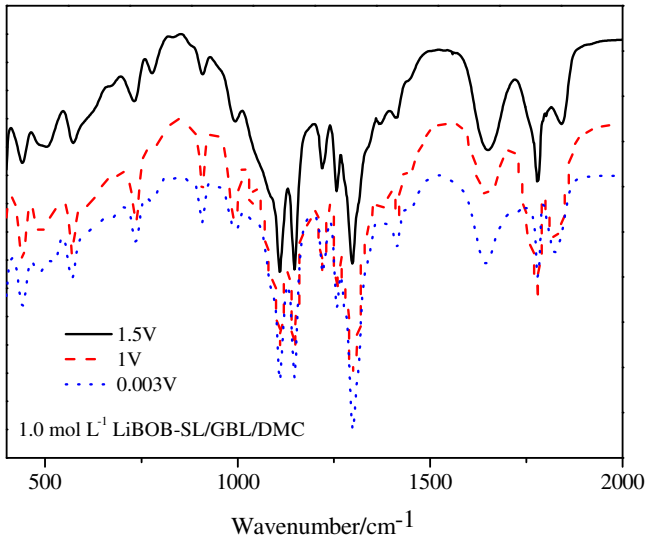

Fig. 10. The FTIR spectra of the SEI layer on the anode material in Li/MCMB cell at different potentials, cycled with 1.0 mol L^{-1} LiBOB–SL/GBL/DMC electrolyte during the initial cycle.

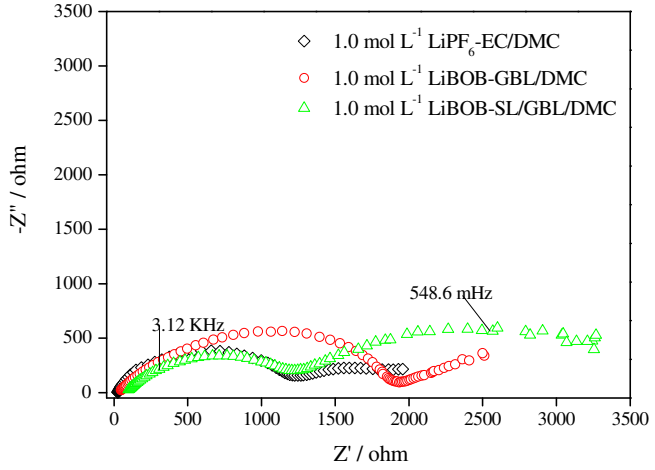

Fig. 11. The EIS spectra of Li/MCMB cells with three electrolytes at 0.003 V during the initial lithiation process at room temperature.

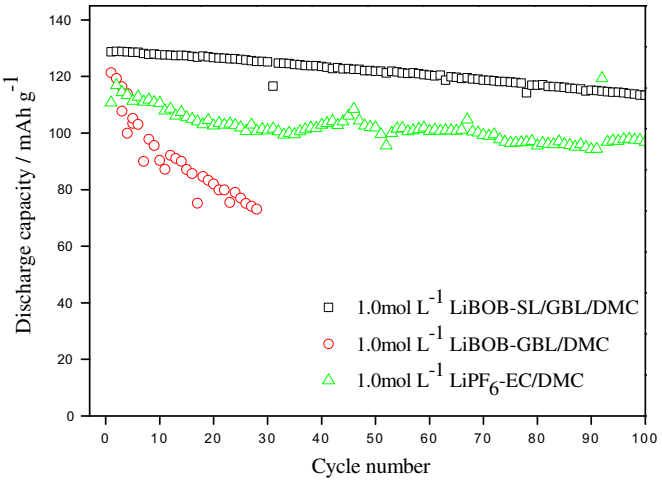

Fig. 12. Cycle performances of $LiNi_{0.5}Mn_{1.5}O_4$/Li cells with different electrolytes with 0.5 C of discharge rate at room temperature, respectively.

shown in Fig. 13, it is obvious that the cell with LiBOB–SL/GBL/DMC electrolyte has higher mean voltage than that of the cell with $LiPF_6$–EC/DMC electrolyte. The reason may be due to the fact that the electrode polarization resistance of the cell with $LiPF_6$–EC/DMC electrolyte is higher than that of the cell with LiBOB–SL/GBL/DMC electrolyte, for the generated HF in $LiPF_6$–EC/DMC electrolyte not only would attack cathode material to make transitional metal to dissolute, but also reacts with conductive components in SEI layer to increase the resistance on anode surface.

3.10. Rate capabilities of $LiNi_{0.5}Mn_{1.5}O_4$/Li cells

The discharge capacities of $LiNi_{0.5}Mn_{1.5}O_4$/Li cells with LiBOB–SL/GBL/DMC and $LiPF_6$–EC/DMC electrolytes are, respectively, tested with different current densities at room temperature (Fig. 14). With the increased discharge rate, the discharge capacity decreases, owing to the increased polarization resistance. As shown in Fig. 14, both of them have similar current discharge capability retentions. It indicates that, though the conductivity of LiBOB–SL/GBL/DMC system is lower than that of $LiPF_6$–EC/DMC system, the rate capability is almost unaffected by the decrease of electrode polarization resistance.

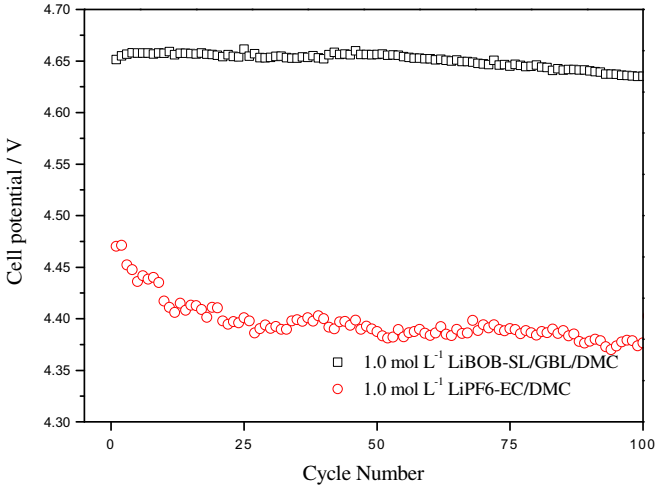

Fig. 13. Mean voltages of $LiNi_{0.5}Mn_{1.5}O_4$/Li cells with two electrolytes with 0.5 C of discharge rate at room temperature, respectively.

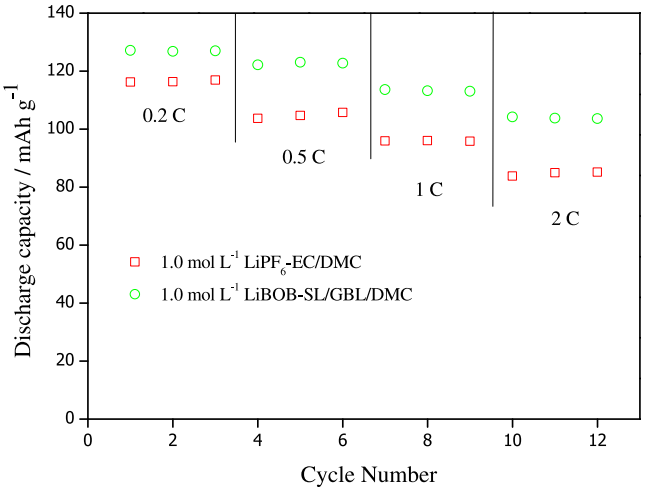

Fig. 14. Discharge capacities of $LiNi_{0.5}Mn_{1.5}O_4$/Li cells with different discharge rates at room temperature, respectively.

4. Conclusions

LiBOB is a promising salt for lithium-ion batteries owing to its unique characteristics. SL and GBL are promising supporting solvents to exert the electrochemical performance of LiBOB. In this study, the electrochemical performances of two novel electrolytes, LiBOB–GBL/DMC and LiBOB–SL/GBL/DMC, are investigated. The results indicate that SL not only improves the stability against oxidative decomposition, but also decreases the electrode polarization resistance. More than that, 1.0 mol L^{-1} LiBOB–SL/GBL/DMC electrolyte shows good compatibilities with both intercalation hosts as cathode and anode. It suggests that the novel electrolyte, 1.0 mol L^{-1} LiBOB–SL/GBL/DMC, would be an alternative electrolyte for 5 V high-voltage rechargeable lithium-ion batteries based upon $LiNi_{0.5}Mn_{1.5}O_4$ cathode.

Acknowledgments

This work was supported by the Science and Technology Planning Project of Gansu Province under contract No. 110RJYA056, the Natural Science Foundation of China under contract No. 20961004 and No. 51002164, and the Fundamental Research Funds for Universities of Gansu Province under contract No. 1105ZTC136. We acknowledge computing resources and time on the Supercomputing Center of Cold and Arid Region Environment and Engineering Research Institute of Chinese Academy of Sciences and Supercomputing Environment of Chinese Academy of Sciences.

References

[1] M. Armand, J.M. Tarascon, Nature 451 (2008) 652–657.
[2] L.W. Ji, Z. Lin, M. Alcoutlabi, X.W. Zhang, Energy Environ. Sci. 4 (2011) 2682–2699.
[3] J.H. Kim, S.T. Myung, C.S. Yoon, S.G. Kang, Y.K. Sun, Chem. Mater. 16 (2004) 906–914.
[4] J. Liu, A. Manthiram, Chem. Mater. 21 (2009) 1695–1707.
[5] L.P. Wang, H. Li, X.J. Huang, E. Baudrin, Solid State Ionics 193 (2011) 32–38.
[6] G.B. Zhong, Y.Y. Wang, Y.Q. Yu, C.H. Chen, J. Power Sources 205 (2012) 385–393.
[7] K. Xu, A.V. Cresce, J. Mater. Chem. 21 (2011) 9849–9864.
[8] A. Caballero, M. Cruz, L. Hernán, M. Melero, J. Morales, E.R. Castellón, J. Electrochem. Soc. 152 (2005) A552–A559.
[9] M. Jo, Y.K. Lee, K.M. Kim, J. Cho, J. Electrochem. Soc. 157 (2010) A841–A845.
[10] X.K. Huang, Q.S. Zhang, J.L. Gan, H.T. Chang, Y. Yang, J. Electrochem. Soc. 158 (2011) A139–A145.
[11] J. Arrebola, A. Caballero, L. Hernán, J. Morales, E.R. Castellón, J.R.R. Barrado, J. Electrochem. Soc. 154 (2007) A178–A184.

[12] D.J. Lee, J. Hassoun, S. Panero, Y.K. Sun, B. Scrosati, Electrochem. Commun. 14 (2012) 43–46.
[13] K. Xu, C.A. Angell, J. Electrochem. Soc. 149 (2002) L7.
[14] Y.A. Lebdeh, I. Davidson, J. Electrochem. Soc. 156 (2009) A60–A65.
[15] Y.S. Zhu, X.W. Gao, X.J. Wang, Y.Y. Hou, L.L. Liu, Y.P. Wu, Electrochem. Commun. 22 (2012) 29–32.
[16] J.Y. Huang, X.J. Liu, X.L. Kang, Z.X. Yu, T.T. Xua, W.H. Qiu, J. Power Sources 189 (2009) 458–461.
[17] K. Xu, J. Electrochem. Soc. 155 (2008) A733–A738.
[18] S.Y. Li, Y.Y. Zhao, X.M. Shi, B.C. Li, X.L. Xu, W. Zhao, X.L. Cui, Electrochim. Acta 65 (2012) 221–227.
[19] B.T. Yu, W.H. Qiu, F.S. Li, L. Cheng, J. Power Sources 158 (2006) 1373–1378.
[20] P. Ping, Q.S. Wang, J.H. Sun, X.Y. Feng, C.H. Chen, J. Power Sources 196 (2011) 776–783.
[21] W.H. Yao, Z.R. Zhang, J. Gao, J. Li, J. Xu, Z.C. Wang, Y. Yang, Energy Environ. Sci. 2 (2009) 1102–1108.
[22] S.Y. Li, B.C. Li, X.L. Xu, X.M. Shi, Y.Y. Zhao, L.P. Mao, X.L. Cui, J. Power Sources 209 (2012) 295–300.
[23] M.J. Frisch, G.W. Trucks, H.B. Schlegel, G.E. Scuseria, M.A. Robb, J.R. Cheeseman, G. Scalmani, V. Barone, B. Mennucci, G.A. Petersson, H. Nakatsuji, M. Caricato, X. Li, H.P. Hratchian, A.F. Izmaylov, J. Bloino, G. Zheng, J.L. Sonnenberg, M. Hada, M. Ehara, K. Toyota, R. Fukuda, J. Hasegawa, M. Ishida, T. Nakajima, Y. Honda, O. Kitao, H. Nakai, T. Vreven, J.A. Montgomery Jr., J.E. Peralta, F. Ogliaro, M. Bearpark, J.J. Heyd, E. Brothers, K.N. Kudin, V.N. Staroverov, R. Kobayashi, J. Normand, K. Raghavachari, A. Rendell, J.C. Burant, S.S. Iyengar, J. Tomasi, M. Cossi, N. Rega, J.M. Millam, M. Klene, J.E. Knox, J.B. Cross, V. Bakken, C. Adamo, J. Jaramillo, R. Gomperts, R.E. Stratmann, O. Yazyev, A.J. Austin, R. Cammi, C. Pomelli, J.W. Ochterski, R.L. Martin, K. Morokuma, V.G. Zakrzewski, G.A. Voth, P. Salvador, J.J. Dannenberg, S. Dapprich, A.D. Daniels, O. Farkas, J.B. Foresman, J.V. Ortiz, J. Cioslowski, D.J. Fox, Gaussian 09, Revision A. 02, Gaussian, Inc, Wallingford CT, 2009.
[24] D. Belov, D.T. Shieh, J. Solid State Electrochem. 16 (2012) 603–615.
[25] Y. Matsuo, K. Fumita, T. Fukutsuka, Y. Sugie, H. Koyama, K. Inoue, J. Power Sources 119 (2003) 373–377.
[26] R.J. Chen, F. Wu, L. Li, Y.B. Guan, X.P. Qiu, S. Chen, Y.J. Li, S.X. Wu, J. Power Sources 172 (2007) 395–403.
[27] D. Aurbach, B. Markovsky, Y. Talyossef, G. Salitra, H.J. Kim, S. Choi, J. Power Sources 162 (2006) 780–789.
[28] S.S. Zhang, J. Power Sources 163 (2007) 713–718.
[29] L.P. Mao, B.C. Li, X.L. Cui, Y.Y. Zhao, X.L. Xu, X.M. Shi, S.Y. Li, F.Q. Li, Electrochim. Acta 79 (2012) 197–201.
[30] S.Y. Li, X.L. Cui, X.L. Xu, X.M. Shi, G.X. Li, Russ. J. Electrochem. 48 (2012) 518–524.
[31] J.Y. Huang, L.Z. Fan, B.T. Yu, T.F. Xing, W.H. Qiu, Ionics 16 (2010) 509–513.
[32] S.C. Kinoshitaa, M. Kotatoa, Y. Sakataa, M. Uea, Y. Watanabeb, H. Morimotob, S.I. Tobishima, J. Power Sources 183 (2008) 755–760.
[33] S.Y. Li, X.L. Xu, X.M. Shi, Y.Y. Zhao, H.M. Zhang, Y.L. Li, W. Zhao, X.L. Cui, L.P. Mao, J. Power Sources 217 (2012) 503–508.
[34] M. Safari, M. Morcrette, A. Teyssot, C. Delacourt, J. Electrochem. Soc. 156 (2009) A145–A153.
[35] M. Matsui, K. Dokko, Y. Akita, H. Munakata, K. Kanamura, J. Power Sources 210 (2012) 60–66.